frontiers in Chemical Engineering

ORIGINAL RESEARCH
published: 28 September 2021
doi: 10.3389/fceng.2021.738643

Creaming Layers of Nanocellulose Stabilized Water-Based Polystyrene: High-Solids Emulsions for 3D Printing

*Marie Gestranius[1], Katri S. Kontturi[1], Atte Mikkelson[1], Tommi Virtanen[1], Claudia Schirp[2], Emily D. Cranston[3], Eero Kontturi[4] and Tekla Tammelin[1]**

[1]*VTT Technical Research Centre of Finland Ltd., Espoo, Finland,* [2]*Fraunhofer Institute for Wood Research, Wilhelm-Klauditz-Institut WKI, Braunschweig, Germany,* [3]*Department of Wood Science, Department of Chemical and Biological Engineering and Bioproducts Institute, The University of British Columbia, Vancouver, BC, Canada,* [4]*Department of Bioproducts and Biosystems, School of Chemical Engineering, Aalto University, Espoo, Finland*

Oil-in-water emulsions stabilized using cellulose nanofibrils (CNF) form extremely stable and high-volume creaming layers which do not coalesce over extended periods of time. The stability is a result of the synergistic action of Pickering stabilization and the formation of a CNF percolation network in the continuous phase. The use of methyl cellulose (MC) as a co-emulsifier together with CNF further increases the viscosity of the system and is known to affect the droplet size distribution of the formed emulsion. Here, we utilize these highly stable creaming layer systems for *in situ* polymerization of styrene with the aim to prepare an emulsion-based dope for additive manufacturing. We show that the approach exploiting the creaming layer enables the effortless water removal yielding a paste-like material consisting of polystyrene beads decorated with CNF and MC. Further, we report comprehensive characterization that reveals the properties and the performance of the creaming layer. Solid-state NMR measurements confirmed the successful polymerization taking place inside the nanocellulosic network, and size exclusion chromatography revealed average molecular weight (M_w) of polystyrene as approximately 700,000 Da. Moreover, the amount of the leftover monomer was found to be less than 1% as detected by gas chromatography. The dry solids content of the paste was ~20% which is a significant increase compared to the solids content of the original CNF dispersion (1.7 wt %). The shrinkage of the CNF, MC and polystyrene structures upon drying—an often-faced challenge—was found to be acceptable for this composite containing highly hygroscopic biobased materials. At best, the two dimensional shrinkage was no more than ca. 20% which is significantly lower than the shrinkage of pure CNF being as high as 50%. The paste, which is a composite of biobased materials and a synthetic polymer, was demonstrated in direct-ink-writing to print small objects. With further optimization of the formulation, we find the emulsion templating approach as a promising route to prepare composite materials.

Keywords: cellulose nanofibrils (CNF), pickering emulsion, creaming layer, methyl cellulose, 3D printing, additive manufacturing, biocomposite, nanocellulose

OPEN ACCESS

Edited by:
Florent Allais, AgroParisTech Institut des Sciences et Industries du Vivant et de L'environnement, France

Reviewed by:
Akira Isogai, The University of Tokyo, Japan
Long Bai, Northeast Forestry University, China

****Correspondence:***
Tekla Tammelin
Tekla.tammelin@vtt.fi

Specialty section:
This article was submitted to Chemical Reaction Engineering, a section of the journal Frontiers in Chemical Engineering

Received: *09 July 2021*
Accepted: *10 September 2021*
Published: *28 September 2021*

Citation:
Gestranius M, Kontturi KS, Mikkelson A, Virtanen T, Schirp C, Cranston ED, Kontturi E and Tammelin T (2021) Creaming Layers of Nanocellulose Stabilized Water-Based Polystyrene: High-Solids Emulsions for 3D Printing. Front. Chem. Eng. 3:738643. doi: 10.3389/fceng.2021.738643

INTRODUCTION

It is universally acknowledged that nanocellulosic materials (cellulose nanocrystals (CNC), cellulose nanofibrils (CNF), cellulose microfibrils (CMF) and bacterial cellulose (BC)) can assemble at oil-water interfaces to act as emulsion stabilizers and are able to provide templates for *e.g.* heterogeneous polymerization (Kedzior et al., 2020). In their natural state, nanocelluloses stabilize oil-in-water emulsions due to their hydrophilic and amphiphilic character via Pickering mechanism. (Ramsden, 1904; Ougiya et al., 1997; Kalashnikova et al., 2011; Lam et al., 2014; Winuprasith and Suphantharika, 2015; Nikfarjam et al., 2015; Gestranius et al., 2017). Specifically, emulsions stabilized by CNF networks tend to form voluminous and highly stable creaming layers via the formation of a percolation network of the long and flexible nanofibrils (Gestranius et al., 2017). Building on our previous findings that mechanically disintegrated CNF from plant-based sources stabilize oil-in-water emulsions against coalescence whilst forming a thick creaming layer, we introduce an approach to prepare a water-based polymer system that is applicable, for example, as an ink in additive manufacturing. Generally, in the context of classical emulsion polymerization, creaming is an unwanted process whereas our approach relies on the strong creaming behavior in order to form high-consistency paste-like suspensions.

Nanocelluloses are widely utilized in heterogeneous water-based polymer systems aiding polymerization processes as reviewed by Kedzior et al., 2020. Procedures to manufacture nanocellulose covered polymer microbeads where nanocellulosic materials have been used as stabilizers of emulsions of non-polar liquid monomers, followed by subsequent polymerization of the monomer have been introduced by Ben Mabrouk et al., 2014, Aymen et al., 2009, Kedzior et al., 2020. These procedures result in polymeric nano- or microbeads decorated with nanocellulosic materials, where the components are bound to each other already at the emulsification step, giving an even distribution of synthetic polymer and biobased materials throughout the sample matrix. Moreover, the droplet size of this process is controllable and depends on many factors; mixing conditions, type of nanocellulose used and monomer solubility in aqueous medial (Gestranius et al., 2017; Jiménez Saelices et al., 2019).

Recently, the use of methyl cellulose (MC) as a co-emulsifier together with CNC was found to have a pronounced effect on the emulsion droplet size (Hu et al., 2015), and by altering the ratios of CNC and MC, the size distribution of the polymerized particles could also be manipulated (Kedzior et al., 2017). Emulsion templating has been used to form a wide range of nanocellulosic composite materials, through casting of films, melt pressing of cast films and formation of foams via high internal phase emulsions and freeze-drying. (Blaker et al., 2009; Ballner et al., 2016; Dastjerdi et al., 2017; Fujisawa et al., 2017; Li et al., 2018). However, their use in additive manufacturing, without further processing is still limited due to the high water content of the final emulsions.

In additive manufacturing, or more commonly 3D printing, 3D objects are built up layer-by-layer, by extrusion of a liquid ink or a melting of a filament. The 3D printable materials should have either suitable viscosity or thermoplasticity depending on the processing method. The advantages of 3D printing are many; it allows complex designs and defining the inner shape of objects, on-demand production, flexibility and fast prototyping, as well as minimum amounts of waste. Recently direct ink writing of emulsion based 3D printing inks, and especially Pickering-stabilized emulsions have been frequently reported in the literature, in several different fields such as hierarchical porous ceramic structures, skin-bearing architectures and bio-active scaffolding (Minas et al., 2016; Huan et al., 2019; Chan et al., 2020; Wang et al., 2021). Nanocellulosic materials thrive in aqueous environments forming highly viscous dispersions, making them potential candidates as inks in 3D printing. Nanocellulosic materials are, indeed, suitable for 3D printing, and have shown great potential in biomedical applications and scaffolding, where the intended use is in the wet state. (Chinga-Carrasco, 2018; Heggset et al., 2019; Mohan et al., 2020). The challenge is to retain the shape of the printed objects, especially upon drying, since 3D printed objects with high water content severely shrink, deform and crack. Many routes have been used to circumvent this such as use of additives, cross-linking or curing, formation of foams, dissolving and regeneration as well as freeze drying (Rees et al., 2015; Voisin et al., 2018; Wang et al., 2018; Mohan et al., 2020; Jiang et al., 2021). Nanocellulosic materials, among other biobased materials, have also been used in 3D printable bionanocomposites, frequently as a component in polymer filaments. However, the poor compatibility between nanocellulosic materials and polymers causes problems, and grafting and chemical modification of the nanocellulosic material is often needed to achieve homogeneous distributions of them in filaments for 3D printing. (Murphy and Collins, 2018; Huang et al., 2019; Mohan et al., 2020). Recently the Pickering emulsion approach was used to form dried beads of polylactic acid (PLA) covered in BC. (Li et al., 2019) The dried beads were processed into 3D printable filaments, which gave an even distribution of BC upon printing of composite materials.

In this work, we present an emulsion templating approach in which the emulsion formation and styrene polymerization take place simultaneously leading to a paste-like material suitable for direct ink writing, see the scheme in **Figure 1**. The formulation is based on the synergistic effect provided by CNF and MC displaying strong creaming behavior. The exploitation of creaming layer allows an effortless water removal—a feature that is clearly differentiating us from the other approaches using Pickering emulsions as polymerization templates or in 3D printing inks (Kedzior et al., 2017; Sommer et al., 2017; Jiménez Saelices et al., 2019; Li et al., 2019). Our procedure overcomes several challenges related to composite materials conjoining aqueous nanocellulose with synthetic polymer: 1) effortless water removal taking place during creaming layer formation enables significant increase in solids content from ~2 wt% up to 20 wt%; 2) uniform distribution of CNF throughout the synthetic matrix is achieved via the formation of a percolated network giving strength and stability to the structure. 3) The use of MC as a co-emulsifier allows us to manufacture polymer beads with an even size distribution.

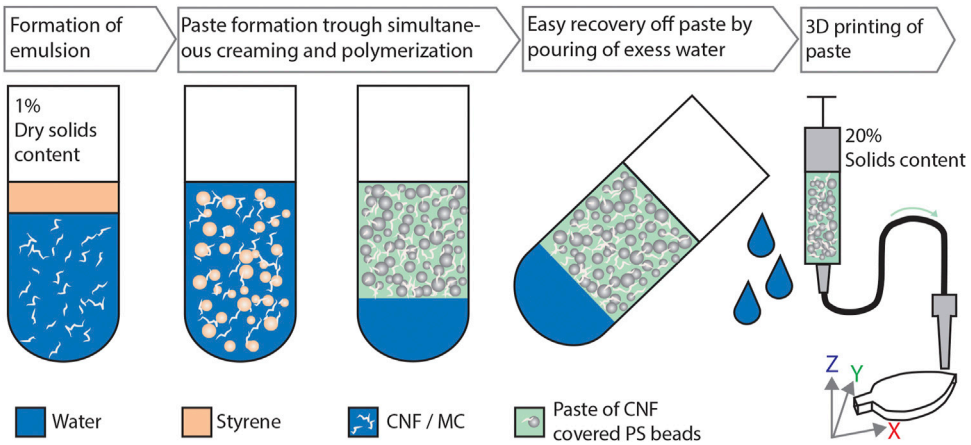

FIGURE 1 | The evolution of mechanically disintegrated CNF, dissolved MC and styrene into a high-solids creaming layer suitable for additive manufacturing prepared via emulsion templating. Simultaneous creaming and polymerization of styrene-in-water emulsion stabilized with CNF and MC forms a paste-like material consisting of polystyrene beads covered with MC and CNF. The distinct two-phase system allows effortless removal of free water.

The structure of the composite creaming layer "pastes" was revealed by SEM imaging, which also elucidated the droplet size distribution via image analysis. The pastes were subjected to chemical characterization using size exclusion chromatography (SEC) for molar mass determination, unreacted monomer content using gas chromatography (GC), as well as solid state NMR to analyze the chemical structure. Shrinkage was quantified to assess the suitability of creaming layers as direct writing inks for 3D printing. While creaming of emulsions is typically an undesired phenomena, this work takes advantage of this phase separation action for the effortless formation of a new high-consistency composite material.

MATERIALS AND METHODS

Mechanically Disintegrated Cellulose Nanofibrils

The same grade of mechanically disintegrated CNF was utilized to produce oil-in-water Pickering emulsions with distinctive creaming layer formation as previously demonstrated and characterised as described in detail in Gestranius et al. (2017). In short, never dried bleached birch kraft pulp, with a carbohydrate content of 73 wt% glucose, 23 wt% xylose, and 0.15 wt% methyl glucuronic acid (from Finnish pulp mill) at 1.7 wt% was dispersed and pre-refined using a grinder (Supermasscolloider MKZA10-15J, Masuko Sangyo Co., Japan) at 1,500 rpm. The CNF gel was produced by passing the pre-refined fiber suspension through a microfluidizer for 5 times (Microfluidics, M-7115-30, Westwood, MA, United States) using Z-type chambers of 500 and 100 μm at the operating pressure of 1800 bar. The final CNF suspension appeared as a turbid gel at 1.7 wt%, presented in **Figure 2Ai**). The width of the fibrils was approximately 10 nm and the length varying from a few micrometer up to 10 µm (Tenhunen et al., 2014). The charge of CNF was ~0.04 mmol g^{-1} as determined by a standard conductometric titration (SCAN-CM 65:02, 2002). Atomic force microscopy (AFM) images of self-standing films of CNF made by solution casting were made to visualize the fibrillar structure, as shown in **Figure 2B**. Images were captured using a Nanoscope IIIa Multimode scanning probe micro-scope (Bruker AXS Inc., Madison, WI, United States) with an E-scanner in tapping mode using NSC15/AIBS silicon cantilevers (Ultrasharp, µmasch, Tallinn, Estonia). No other image processing except flattening was performed.

Chemicals

Styrene was purchased from Sigma-Aldrich (S4972 ReagentPlus®, purity ≥99%) and used without further modification. An initiator, 2,2-azobis-isobutyronitrile (AIBN) (441,090, 98%) was purchased from Sigma-Aldrich, and purified by recrystallization from chloroform. Methyl cellulose (Sigma-Aldrich, M0512), with a low molecular weight, 88,000 Da, and a degree of substitution of 1.5–1.9 as given by the producer, was used as received. D-sorbitol (Sigma-Aldrich, S1876) was dissolved in Milli-Q water to a 50 wt% solution.

Preparation of Pastes

Preparation of CNF and MC Dispersions

Methyl cellulose was selected as a co-emulsifier, to increase the viscosity in 3D printing and due to its ability to regulate emulsion droplet sizes (Hu et al., 2015; Kedzior et al., 2017). First the aqueous phases containing different ratios of CNF and MC were prepared. CNF was diluted into 34 ml Milli-Q water at the concentrations given in **Table 1**. The ratios were chosen to represent samples stabilized by only MC, mostly by MC, equal amounts of CNF and MC, mostly by CNF and only by CNF. Efficient mixing of dispersions was partially limited by the high viscosity, explaining the different wt% of MC and CNF. The diluted dispersions were heated to approximately 80°C in a water bath. MC was added as a powder according to concentrations given in **Table 1**, to the heated dispersions and mixed until well

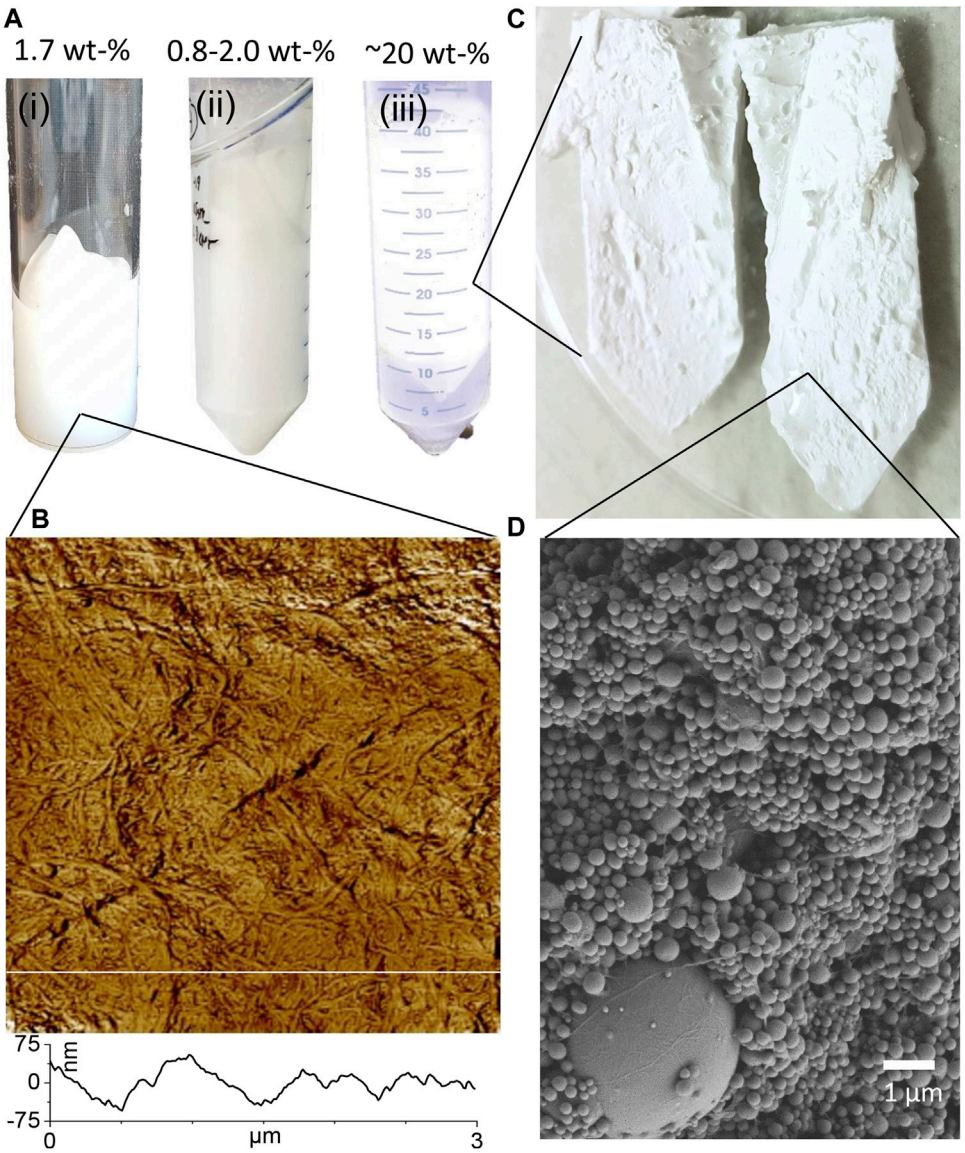

FIGURE 2 | (A) Photographs of (i) mechanically disintegrated CNF gel, (ii) freshly prepared emulsion (iii) and polymerized emulsion. **(B)** 3 × 3 µm AFM phase contrast image of CNF fibrils, and graph of height profile corresponding to segment line. (AFM height contrast image available in **Supplementary Figure S1**). **(C)** Photograph of creaming layer cut into two halves after discarding the excess water. **(D)** SEM image of the structure of the dried creaming layer containing only CNF (CNF100).

TABLE 1 | Concentrations of aqueous dispersions of CNF and MC and their corresponding Brookfield viscosities at rotational speeds of 0.5 and 10 rpm. The sample name indicate the ratio of the two stabilizers CNF and MC.

Sample	Concentration (wt%)		Spindel	Viscosity (mPas)	
	CNF	MC		0.5 rpm	10 rpm
MC100	0.00	2.35	V72	10,500 ± 200	8,790 ± 40
CNF13MC87	0.26	1.76	V72	7,770 ± 0	5,030 ± 30
CNF50MC50	0.74	0.73	V71	8,300 ± 100	1,323 ± 7
CNF83MC17	0.74	0.15	V71	4,400 ± 800	340 ± 30
CNF100	1.05	0.00	V73	48,000 ± 200	2,100 ± 200

TABLE 2 | Dry thought ratios of the components of the emulsions, excluding water.

Sample	Concentration (wt%)			
	CNF	MC	Styrene	AIBN
MC100	0.00	12.83	87.00	0.17
CNF13MC87	1.45	9.78	88.60	0.17
CNF50MC50	4.24	4.19	91.39	0.18
CNF83MC17	4.39	0.89	94.54	0.19
CNF100	6.17	0.00	93.65	0.18

dispersed. The dispersions containing CNF and MC were cooled during mixing until no visual aggregates of undissolved MC remained, and were stored at 8°C for a minimum of 12 h before characterization or further use in emulsions. The CNF/MC dispersions were all gel like. Sample MC100 containing only MC was clear, while the samples containing CNF were translucent.

Characterization of CNF/MC Dispersions Prior to Emulsification

The shear viscosity of each CNF/MC dispersions before addition of styrene was measured at room temperature using a Brookfield Rheometer RVDV-III Ultra (Brookfield AMETEK Inc. Middleboro, MA, United States) in a similar way as in work presented by Kangas et al. (Kangas et al., 2014). Data of the viscosity at 0.5 rpm were collected at 300 measuring points and at 10 rpm at 180 measuring points. Different sized spindels of Vane type were used in the measurements depending on the viscous nature of the sample. Presented data in **Table 1** is the average of the last five data points at series, of two parallel measurements. The Brookfield viscosities measured at two different speeds, decrease more at 10 rpm for sample with a higher concentration of CNF, indicating a stronger shear thinning behavior typical for CNF (Klemm et al., 2011; Honorato et al., 2015).

Emulsification and Polymerization of CNF/MC/Styrene Dispersions

The initiator AIBN (0.0107 g) was added to 6 ml of styrene and dissolved by gentle stirring in a vial. 34 ml of dispersions with different ratios of CNF/MC given **Table 1**, were mixed using a sonicator (Branson Digital Sonifier, 400 W; 20 kHz) at 25% amplitude for 5 min in an ice bath. Styrene, containing dissolved AIBN, was added to the dispersion and a pre-emulsion was formed through vigorous shaking of the closed test tube. Emulsions were prepared by mixing with the sonicator using pulses of 0.5 s followed by pauses of 0.5 s. First with an active mixing time of 1 min at 60% amplitude followed by an active mixing time of 1 min at 70% amplitude, at atmospheric conditions, while cooled in an ice bath. The ratios of dry components in the emulsions are presented in **Table 2**. For polymerization of the styrene, the formed emulsions were placed in closed test tubes in an oven at 80°C for 24 h, without stirring. After cooling, excess water was drained away, leaving a paste. The pastes were processed at high shear by passing between two 10 ml plastic syringes connected with an adapter, until running smoothly. A syringe was then adapted with 3D printing nozzles and the paste was passed through decreasing nozzle sizes, to sieve the paste for printing. For dry solids content determination, a small amount of paste was put in an aluminum pan and dried in the oven over night at 105°C. Dry solids content was calculated from two parallels. The dry solids content of the processed pastes was around 20 wt% for most of the pastes, as given in **Table 3**. The comparably lower dry solids content around 15 wt% of sample MC100 and CNF50MC50 can probably be explained by some excess water left in the tube before draining. Visually there were no obvious differences between the samples regardless of the stabilizer ratio.

Characterization of Pastes—Morphology and Chemistry

Scanning Electron Microscopy and Image Analysis

Scanning electron microscopy (SEM) (Zeiss FE-SEM Merlin, Germany) was used to evaluate the structure of the pastes. A thin layer of paste was put on SEM holders using a spatula and dried at ambient room conditions for 24 h. A 2 nm layer of gold palladium layer was coated with a sputter coater (EM ACE200 Leica, Germany) prior to SEM imaging. The specimens were analyzed using SEM from at least two locations per sample and with 1,000, 5,000, and 10000× magnifications. The 1,000× magnification images were used to measure the size of all larger beads (approximately ø>1 μm), with a clearly visible diameter, using the ImageJ software. Due to overlapping beads no suitable threshold was found for automatic image analysis and the measurements were made manually in ImageJ. The population size consisting of numbers of particles measured and mean diameters with standard deviation were noted.

Gas Chromatography

Remaining unreacted styrene of the creaming layers was analyzed by using gas chromatography. Ca. 100 mg of paste was weighed accurately and placed in a measuring bottle containing 10 ml of acetone and filtered. 100 μL solution was pipetted into 20 ml of headspace vial and closed. Sample vials were first incubated for 30 min at 50°C, and then 1 ml of gas phase was injected (split mode; 225°C; split flow of 30:1) into a gas chromatograph equipped with a flame ionization detector (HS-GC-FID) and headspace autosampler

TABLE 3 | Dry solids content and shrinkage of samples with increasing CNF content *)Reference sample, CNF hydrogel.

Sample	MC100	CNF13MC87	CNF50MC50	CNF83MC17	CNF100	Ref*)
Dry solids content (%)	16.1	22.6	14.9	20.5	20.7	1.7
Shrinkage, line (%)	2.6	6.6	6.1	14.8	18.5	14.7
Shrinkage, square (%)	11.4	19.0	27.9	45.3	42.3	51.0

(Agilent 7,890 Series; Palo Alto, CA, United States). The carrier gas was helium (constant flow of 1.4 ml min^{-1}) and HP-5 capillary column, 50 m × 0.32 mm × 1.05 μm (J&W Scientific, Folsom, CA) was applied. The temperature profile was 50°C for 3 min, increased to 100°C by 10°C min^{-1}, to 140°C by 5°C min^{-1} and to 260°C by 15°C min^{-1}, followed by isothermal conditions for 1 min. Compound identification was done by comparing authentic standard (styrene ≥99%, Sigma) and quantified with a standard curve.

Size Exclusion Chromatography

The molar mass measurements of the creaming layers were performed with size exclusion chromatography (SEC) using chloroform as eluent. The pastes, were dissolved overnight in chloroform (concentration of 1–5 mg/ml). In all cases the samples were filtered (0.45 μm) before the measurement. The SEC measurements were performed in chloroform eluent (0.6 ml/min, T = 30°C) using Styragel HR 4 and 3 columns with a pre-column. The elution curves were detected using Waters 2414 refractive index detector. The molar mass distributions (MMD) were calculated against 10 × PS (580–3,040,000 g/mol) standards, using Waters Empower 3 software.

Solid-State NMR

Solid-state NMR was performed on the creaming layer CNF50MC50, which was air-dried and crushed to a powder. The ^{13}C cross polarization (CP) magic angle spinning (MAS) NMR measurement was performed using an Agilent DD2 600 NMR spectrometer (Santa Clara, United States) with magnetic flux density of 14.1 T, equipped with a 3.2 mm T3 MAS NMR probe operating in a double resonance mode. The sample was packed in ZrO_2 rotors, MAS rate in the experiment was set to 10 kHz. 16,000 scans were accumulated using a 1.3 ms contact time and a 3.0 s delay between successive scans. Protons were decoupled during acquisition using SPINAL-64 proton decoupling with a field strength of 80 kHz. 90° pulse durations and Hartmann-Hahn match for cross polarization were calibrated using α-glycine. The chemical shift scale was externally referenced to adamantane signal at 38.48 ppm. All processing was carried out using TopSpin 3.6 software.

3D Printing Using Direct Ink Writing

Shrinkage Assessment

Before 3D printing, tests were done manually using syringes equipped with nozzles of 0.84 mm. Objects with defined shapes; a 0.5 × 0.5 cm square and a 3 cm long line; were covered with paste and allowed to dry in a fume hood. The shrinkage was evaluated from measurements using the ImageJ software. The lengths of the lines were manually measured in the software, leaving out cracks and with adjustment of out of line sections. The area of the squares was measured by the software by applying a suitable threshold to the image. Shrinkage of the line was calculated according to **Eq. 1**:

$$Shrinkage_l = \frac{l_{wet} - l_{dry}}{l_{wet}} \times 100 \qquad \text{(Equation 1)}$$

TABLE 4 | Leftover styrene in the pastes, M_n (number average molar mass), Mw (weight average molar mass) and PD (dispersity, M_w/M_n) of the samples with increasing CNF content.

Sample	Styrene (wt%)	M_n (g mol^{-1})	M_w (g mol^{-1})	PD
MC100	0.21 ± 0.01	216,000	742,000	3.4
CNF13MC87	0.37 ± 0.01	243,000	792,000	3.3
CNF50MC50	0.74 ± 0.04	174,000	673,000	3.9
CNF83MC17	1.07 ± 0.03	173,000	682,000	4.0
CNF100	0.75 ± 0.04	176,000	710,000	4.0

Where l stands for the measured length. The shrinkage of the squares was calculated using **Eq. 2**, where A stands for the measured area.

$$Shrinkage_A = \frac{A_{wet} - A_{dry}}{A_{wet}} \times 100 \qquad \text{(Equation 2)}$$

3D Printing of Paste

A proof of concept object was printed with direct ink writing using an Envision 3D bioplotter (Envisiontec, Gladbeck, Germany) using the composition of sample CNF13MC87 (**Table 1**) with the addition of 10% sorbitol of the dry solids weight of the paste. A decorative leaf contour with maximum base dimensions of 2 × 3 cm and a height of 0.5 cm was filled with a diagonal mesh with 4 mm intervals. Parafilm (Bemis Company, United States Neenah, WI) was used as a substrate and the printed leaf was dried at 50% RH for 24 h. Printer speed was 10 mm/s and a pressure of 0.9 bar was used to extrude the sample through a 0.84 mm diameter nozzle.

RESULTS

Appearance and Morphology of Emulsions

CNF and MC underwent several steps on the way toward becoming a creaming layer suitable to be used as a paste for 3D printing. **Figure 1** depicts the process, starting form CNF and MC dispersions, followed by CNF and MC stabilized emulsions of styrene-in-water, and finally becoming a creaming layer consisting of polystyrene beads covered with and bound together by CNF and MC. The viscosity and dry solids content of the CNF/MC dispersions tested are given in **Table 1**. While the total amount of stabilizer certainly affects the emulsion properties, the ratio of the different stabilizers and starting viscosity of the system are also important parameters. Compared to our previous work, even the lowest CNF concentration used in this work is higher than the minimum concentration needed to form stable dodecane-in-water emulsions (Gestranius et al., 2017). Therefore, it was concluded that once the CNF concentration is high enough to stabilize the emulsion, increasing concentrations further seemed to narrow the droplet size distribution, but had less impact on the average droplet size (Gestranius et al., 2017). In general, it can be assumed that once the concentration of Pickering stabilizers is

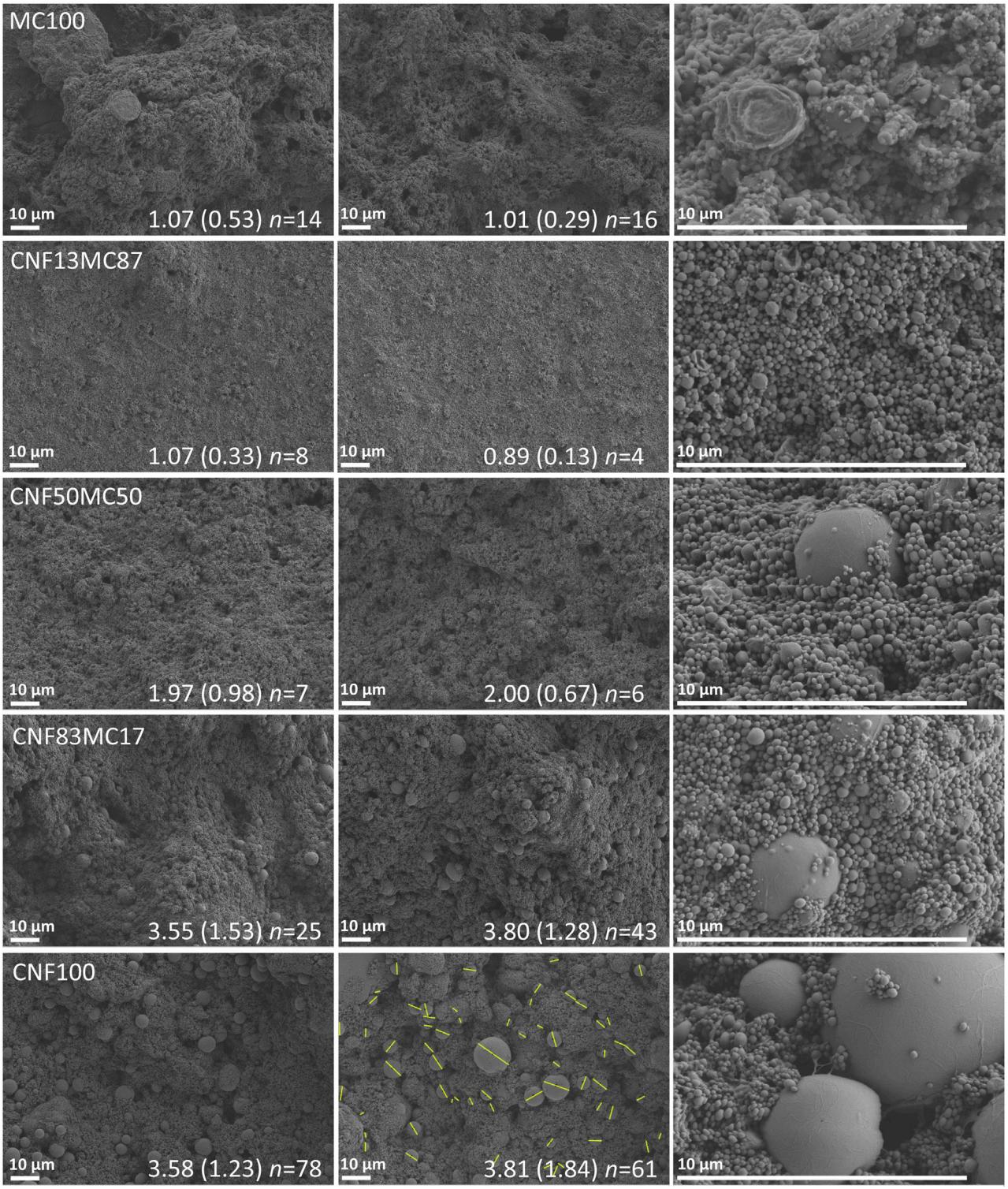

FIGURE 3 | SEM images of the dried creaming layers providing the mean bead diameters of the polystyrene beads (the **left** and the **middle** column). Particle size of the larger polystyrene bead fraction has been evaluated from two representative SEM images of 100,00× magnification in which the smaller bead fraction appears as a blurry background. The inserts give the size of the larger bead fraction presented as "mean diameter, µm (standard deviation) n = number of measured beads". Larger magnification images in the **right** side column depict the structure of the smaller bead fraction. The yellow lines in the center image on the CNF100 row are shown as an illustrative example of the size measurement of the larger bead fraction.

high enough, it will have less effect on particle size of the emulsion (Frelichowska et al., 2010).

Upon extensive mixing CNF/MC dispersions with styrene, styrene-in water emulsions were formed as displayed in **Figure 2A**. The emulsions did not show any signs of instability such as oiling off or droplet coalescence. After the styrene phase was polymerized, two distinct phases appeared, a paste-like creaming layer, and an easily extractable lower water phase (**Figure 2A**). The main component of the polymerized creaming layers is polystyrene (>87 wt%), based on the assumption that the ratios of MC, CNF and styrene (**Table 2**) remain the same after polymerization.

The creaming layers formed by polymerized emulsions stabilized by different ratios of CNF and MC were of high consistency with a final dry solids content of approximately 20 wt% (**Table 3**). The increase in solids content is indeed significant since the original solids content of the CNF/MC dispersion was below 2 wt% (**Table 1**). The conversion rate of polystyrene, based on measurements of unreacted styrene (**Table 4**) was high, >99%. Compared to industrial latexes which often have a dry solids content higher than 40 wt% the dry solids content of the creaming layer is low, however, they remain liquid at high dry solids content. Gelation is known to strongly affect the viscosity and structure of CNC and polysaccharide dispersions, and this is probably also the main mechanism behind the high consistency creaming layer as MC interact with CNF, affecting the network formation and ability of CNF to adsorb at the monomer water interface (Hu et al., 2014). As demonstrated in **Figure 2C**, the pastes are solid enough that they can be easily split in half while retaining their original shape. According to the SEM images, the creaming layer consisted of polystyrene beads, and a percolated network of fibrils (**Figure 2D**). The formation of a stable paste-like creaming layer is highly dependent on the presence of one or both components, MC and CNF, as visually evidenced by photographs shown in the **Supplementary Material** Section 2, and as previously demonstrated by Kedzior et al., 2017.

As MC is significantly more surface active than CNF, it can be presumed that MC takes the role as a main stabilizer (Nasatto et al., 2015). Regardless of the ratios of the stabilizers (**Table 1**), the creaming behavior that leads to the formation of the paste-like material, was always observed. However, the structure of the creaming layer was highly dependent on the CNF/MC ratio as shown in **Figure 3**. Interestingly, with an increasing CNF ratio, there seemed to be more large polystyrene beads present, and a dual size distribution of the beads. The smaller size beads, approximately 0.1–0.3 μm in diameter, was observed regardless of stabilizer ratios and appear even if CNF or MC alone stabilize the emulsion. The larger beads appearing in samples rich in CNF have diameters of approximately 1–10 μm, as given in the insets in **Figure 3**, and are covered with CNF. The dual size distribution of polystyrene particles correlates well with a study where MC and CNC were used as used as latex stabilizers in microsuspension polymerization (Kedzior et al., 2017). It has been suggested–and it is evident—that MC adsorbs on the surface of CNC, giving a synergistic stabilization effect (Hu et al., 2015). Given the similarities of CNC and CNF, this is plausible also in this study, although the adsorption of MC to CNF has not been explicitly investigated. Interestingly, the sample stabilized by CNF alone (no MC) had some smaller polymer beads, implying that CNF is acting as a Pickering stabilizer. This is in contrast to the findings by Kedzior et al. (Kedzior et al., 2017), where the smallest particles were believed to be stabilized by MC alone and the combination of CNC + MC was needed to produce the larger microparticle fraction. As the mechanically produced CNF used in this study is a much more heterogeneous material compared to CNC and emulsions stabilized by them have rather different properties, it is likely that the synergetic effects between CNF and MC are also different (Jiménez Saelices and Capron, 2018).

Another explanation for the presence of the smaller polystyrene beads is that they are initiator stabilized. In two recent studies on systems similar to ours, CNC was used alone to stabilize monomer emulsions containing AIBN as initiator; the two droplet size distributions, one in the nanoscale range and the other one in microscale, were also observed and attributed to the partial water solubility of AIBN allowing for the nucleation and stabilization of nano-latexes (Jiménez Saelices et al., 2019; Glasing et al., 2020). These works suggested that the larger beads are produced via the suspension polymerization mechanism whereas the smaller particles arise from surfactant-free emulsion polymerization stabilized by AIBN. These works highlighted that the initiator choice strongly affected the final sample morphology (Jiménez Saelices et al., 2019; Glasing et al., 2020); when we replaced AIBN with ammonium persulfate (APS) a creaming layer was formed, but the consistency was much too hard for processing into a 3D printing paste (**Supplementary Material** Section 3).

The dual particle size distribution (**Figure 3**) is less pronounced in the samples MC100 (without CNF) and CNF13MC87. The population of the larger beads is the smallest in CNF13MC87 with only 4 and 8 beads compared to the population sizes of 78 and 61 in CNF100. Also the mean bead diameter of the larger bead fraction reported as inserts in **Figure 3**, is considerably smaller in CNF13MC87, 1.07 and 0.89 μm compared to corresponding values of 3.58 and 3.81 μm for the CNF100 sample. Even though the larger beads in samples rich in CNF are still far smaller than the nozzles used in direct ink writing, and should not cause clogging, the smaller, homogeneous size distribution of the beads in sample CNF13MC87 made it the most interesting candidate for 3D printing. MC clearly gives emulsions with more uniform properties, but interestingly the addition of small amounts of CNF will not affect the droplet size distribution, but strengthen the creaming layers via percolation, showing the efficiency of even a low dosage of the nanomaterial.

Evaluation of Polystyrene Formation

The success of the styrene polymerization in an aqueous CNF/MC matrix was confirmed by using solid state NMR spectroscopy. The ^{13}C NMR spectrum in **Figure 4** shows the signals corresponding polystyrene aromatic quaternary carbons (138–148 ppm), protonated aromatic carbons (120–132 ppm), and -CH- and -CH_2- carbons in the polymer backbone (30–50 ppm) (Conte et al., 2007). The weak signals at 66–105 ppm are from carbohydrate carbons of CNF (Moreira et al., 2015), partially overlapped by one spinning side band

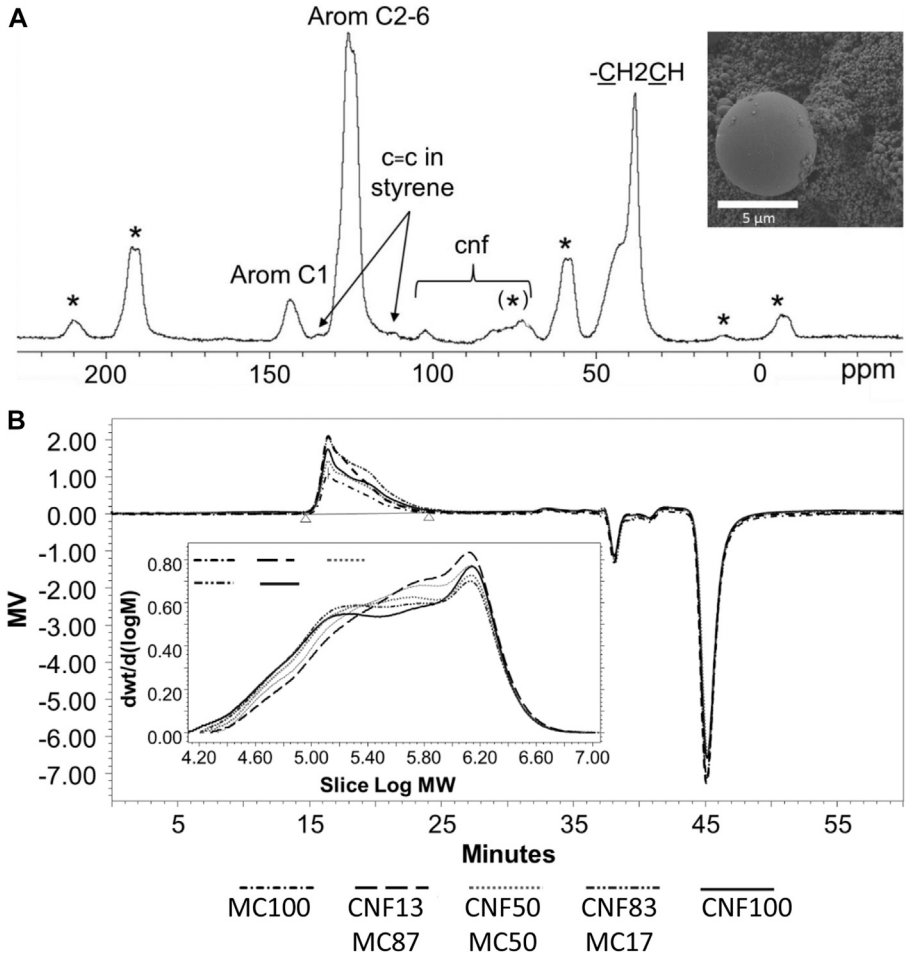

FIGURE 4 | (A): ^{13}C NMR spectrum of the sample CNF50MC50 showing the formation of polystyrene. **(B)**: SEC chromatograms of all samples listed in **Table 4**. The insert shows the molar mass distributions of the corresponding samples.

(marked in the spectrum with asterisks). At 112 and 134 ppm there are two very weak signals which do not belong to polystyrene spectrum. These are likely due to styrene monomer olefinic double bond carbons, for which liquid state ^{13}C NMR signals have been reported to appear at 113.7 and 137.0 ppm.

GC was used to quantify the amount of leftover styrene. It showed that there were only minor amounts of unreacted styrene left in the samples, in most cases less than 1% of the whole sample, as listed in **Table 4**. Sample MC100 and CNF13MC87 had the lowest styrene content with less than 0.4%.

The molecular weight of polystyrene was analyzed by SEC (**Figure 4**), and was found to range from 170,000–250,000 g/mol. Samples MC100 and CNF13MC87 had a higher molecular weight compared to the ones of CNF50MC50, CNF83MC17, and CNF100 and they were also less polydisperse. This could possibly be related to the two different particle size fractions appearing with growing CNF concentrations, indicating a lower molecular weight of the larger beads, giving higher dispersity values. A possible explanation for this could be the two different polymerization mechanisms occurring simultaneously as suggested by Jiménez Saelices et al. and Glasing et al. (Jiménez Saelices et al., 2019; Glasing et al., 2020)

Shrinkage Assessment of Paste-Like Material

Table 3 collects the shrinkage results for manually extruded shapes of the creaming layers with different CNF/MC ratios. The two dimensional shrinkage of sample MC100 (no CNF) was the lowest at 11.4%. With the increasing CNF content, the shrinkage increased form 19.0% to over 40%, along with increasing cracking upon drying. However, shapes manually made from MC100 did not retain their shape in wet state, (**Supplementary Figure S2**). Already a small addition of CNF, as can be observed from the appearance of the sample CNF13MC87, dramatically increased the ability of the paste to retain its shape in the wet state as displayed in **Figure 5A**. The reference sample, pure CNF gel, deformed into a flat film upon drying, and was outperformed by all pastes, as the increased dry

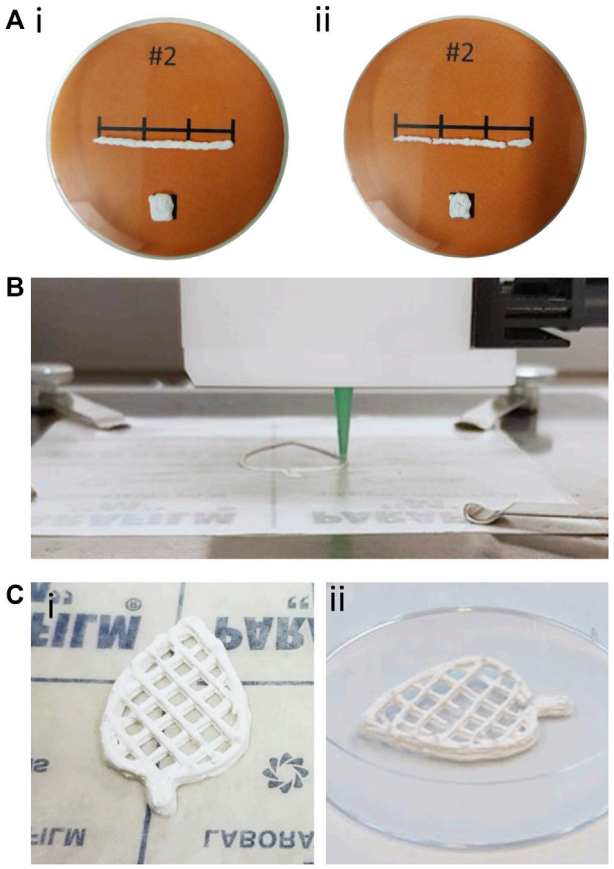

FIGURE 5 | (A) Manually extruded line and square of sample CNF13MC87 (i) before and (ii) after drying. **(B)** 3D printing of the contour of a leaf. **(C)** Photographs of the 3D printed leaf structure (i) in wet state and (ii) after drying.

solids content of the paste is significantly higher than the one of CNF gel (**Figure 2A**). During processing, samples with higher CNF concentrations tended to clog the nozzles, possibly due to the presence of the larger beads, or aggregates of CNF. It can be concluded that the sample CNF13MC87 performed best, regarding its ability to retain shape in wet state, while having the smallest shrinkage of the CNF containing samples. As indicated by the SEM images in **Figure 3**, pastes stabilized by MC or mostly MC have a finer and more uniform bead size distribution, making them preferable for 3D printing.

Proof of Concept in Direct Ink Writing

Sample morphology revealed by SEM (**Figure 3**) as well as the shrinkage assessment results (**Table 3**) both indicate that a small amount of CNF is highly beneficial when optimizing sample properties for 3D printing. This is not surprising since the positive effects of nanomaterials often can be seen at low addition levels. To provide proof of concept, the sample CNF13MC87 was tested in direct ink writing of a demonstrator, after the addition of a small amount of sorbitol for plasticization and softening. The printing process can be seen in **Figure 5B** and the finished proof of concept in the shape of a decorative leaf is displayed in **Figure 5C**. The printing was smooth and the sample retained its shape in the wet state whereas after drying minor deformation and cracks were observed (**Figure 5C**). Considering that the demonstrator is made of a polymerized creaming layer with only a small addition of softener it can be stated that the paste indeed is applicable in direct ink writing. Further optimization of the ink formulation by use of other additives such as clays and tuning of drying conditions could probably improve the performance further, and would be needed for printing of larger objects. However, the efforts to fully optimize the 3D printing system was not within the scope of the current work.

CONCLUSION

Mechanically disintegrated CNF along with MC stabilize styrene-in-water emulsions against coalescence via Pickering mechanism whilst forming a voluminous creaming layer. The aqueous creaming layer system was used for *in situ* polymerization of styrene with high styrene conversion rate (>99%) to prepare composite material conjoining biobased nanocellulose with synthetic polymer. It is worth noting that the use of styrene as a model system is motivated since it is an extensively studied monomer also in emulsion systems stabilized with nanocellulosic materials (Du et al., 2017; Werner et al., 2017; Zhang et al., 2017). The formation of creaming layer facilitated the effortless water removal yielding a high solids "paste" suitable to process 3D printable objects. At best, a tenfold increase in solids content was achieved. Even a low dosage of CNF (0.26 wt%) provided strength and stability for the creaming layer due to the formation of the percolated network whereas MC provided homogeneity with respect to even size distribution of the formed polystyrene beads. The formed paste proved to be 3D printable, and retained its shape upon drying relatively well with the two dimensional shrinkage being approximately 20%.

DATA AVAILABILITY STATEMENT

The raw data supporting the conclusion of this article will be made available by the authors, without undue reservation.

AUTHOR CONTRIBUTIONS

MG carried out the main part of the experimental work, collected and interpreted all the results and wrote the first version of the MS. KSK carried out the initial screening of emulsion formulations and took part in writing of the MS. AM carried out the GC and SEC analysis and wrote the corresponding part of the MS. TV performed the solid-state NMR experiments and wrote the corresponding part of the MS. EC contributed to the materials selection and provided expertise on the utilisation of MC as a co-emulsifier and on the selection of the initiator. CS assisted and carried out the work

related to the reference emulsion systems with different initiators involving the mini-emulsion technique. EK took part in the experimental planning and carefully revised the MS. TT initiated the study concept, took part in the experimental planning, supervised the analysis, critically reviewed the results and conclusions and contributed to the finalization of the manuscript. All listed authors contributed to, read and approved the manuscript.

FUNDING

The work leading to this article has been made in the ValBio-3D project funded by the Academy of Finland via the ERANet-LAC program, and partially in the FireCellCoat project funded by the Ministry of Agriculture and Forestry of Finland via the BIOECONOMY IN THE NORTH program. The work is a part of the Academy of Finland's Flagship Programme under Projects No. 318890 and 318891 (Competence Center for Materials Bioeconomy, FinnCERES). KSK acknowledges Academy of Finland project 310943 for funding.

ACKNOWLEDGMENTS

Adina Anghelescu-Hakala (VTT) is acknowledged for assistance on in-house polymerization practices. Panu Lahtinen (VTT) and Hannes Orelma (VTT) are acknowledged for their assistance on 3D printing.

SUPPLEMENTARY MATERIAL

The Supplementary Material for this article can be found online at: https://www.frontiersin.org/articles/10.3389/fceng.2021.738643/full#supplementary-material

REFERENCES

Ballner, D., Herzele, S., Keckes, J., Edler, M., Griesser, T., Saake, B., et al. (2016). Lignocellulose Nanofiber-Reinforced Polystyrene Produced from Composite Microspheres Obtained in Suspension Polymerization Shows Superior Mechanical Performance. *ACS Appl. Mater. Inter.* 8, 13520–13525. doi:10.1021/acsami.6b01992

Blaker, J. J., Lee, K.-Y., Li, X., Menner, A., and Bismarck, A. (2009). Renewable Nanocomposite Polymer Foams Synthesized from Pickering Emulsion Templates. *Green. Chem.* 11, 1321–1326. doi:10.1039/b913740h

Chan, S. S. L., Sesso, M. L., and Franks, G. V. (2020). Direct Ink Writing of Hierarchical Porous Alumina-stabilized Emulsions: Rheology and Printability. *J. Am. Ceram. Soc.* 103, 5554–5566. doi:10.1111/jace.17305

Chinga-Carrasco, G. (2018). Potential and Limitations of Nanocelluloses as Components in Biocomposite Inks for Three-Dimensional Bioprinting and for Biomedical Devices. *Biomacromolecules* 19, 701–711. doi:10.1021/acs.biomac.8b00053

Conte, P., Carotenuto, G., Piccolo, A., Perlo, P., and Nicolais, L. (2007). NMR-investigation of the Mechanism of Silver Mercaptide Thermolysis in Amorphous Polystyrene. *J. Mater. Chem.* 17, 201–205. doi:10.1039/b613228f

Dastjerdi, Z., Cranston, E. D., and Dubé, M. A. (2017). Synthesis of Poly(n -butyl Acrylate/methyl Methacrylate)/CNC Latex Nanocomposites via *In Situ* Emulsion Polymerization. *Macromol. React. Eng.* 11, 1700013. doi:10.1002/mren.201700013

Du, W., Guo, J., Li, H., and Gao, Y. (2017). Heterogeneously Modified Cellulose Nanocrystals-Stabilized Pickering Emulsion: Preparation and Their Template Application for the Creation of PS Microspheres with Amino-Rich Surfaces. *ACS Sustain. Chem. Eng.* 5, 7514–7523. doi:10.1021/acssuschemeng.7b00375

Elmabrouk, A. B., Wim, T., Dufresne, A., and Boufi, S. (2009). Preparation of Poly(styrene-Co-hexylacrylate)/Cellulose Whiskers Nanocomposites via Miniemulsion Polymerization. *J. Appl. Polym. Sci.* 114, 2946–2955. doi:10.1002/app.30886

Frelichowska, J., Bolzinger, M.-A., and Chevalier, Y. (2010). Effects of Solid Particle Content on Properties of O/w Pickering Emulsions. *J. Colloid Interf. Sci.* 351, 348–356. doi:10.1016/j.jcis.2010.08.019

Fujisawa, S., Togawa, E., and Kuroda, K. (2017). Facile Route to Transparent, Strong, and Thermally Stable Nanocellulose/Polymer Nanocomposites from an Aqueous Pickering Emulsion. *Biomacromolecules* 18, 266–271. doi:10.1021/acs.biomac.6b01615

Gestranius, M., Stenius, P., Kontturi, E., Sjöblom, J., and Tammelin, T. (2017). Phase Behaviour and Droplet Size of Oil-In-Water Pickering Emulsions Stabilised with Plant-Derived Nanocellulosic Materials. *Colloids Surf. A: Physicochemical Eng. Aspects* 519, 60–70. doi:10.1016/j.colsurfa.2016.04.025

Glasing, J., Jessop, P. G., Champagne, P., Hamad, W. Y., and Cunningham, M. F. (2020). Microsuspension Polymerization of Styrene Using Cellulose Nanocrystals as Pickering Emulsifiers: On the Evolution of Latex Particles. *Langmuir* 36, 796–809. doi:10.1021/acs.langmuir.9b03583

Heggset, E. B., Strand, B. L., Sundby, K. W., Simon, S., Chinga-Carrasco, G., and Syverud, K. (2019). Viscoelastic Properties of Nanocellulose Based Inks for 3D Printing and Mechanical Properties of CNF/alginate Biocomposite Gels. *Cellulose* 26, 581–595. doi:10.1007/s10570-018-2142-3

Honorato, C., Kumar, V., Liu, J., Koivula, H., Xu, C., and Toivakka, M. (2015). Transparent Nanocellulose-Pigment Composite Films. *J. Mater. Sci.* 50, 7343–7352. doi:10.1007/s10853-015-9291-7

Hu, Z., Cranston, E. D., Ng, R., and Pelton, R. (2014). Tuning Cellulose Nanocrystal Gelation with Polysaccharides and Surfactants. *Langmuir* 30, 2684–2692. doi:10.1021/la404977t

Hu, Z., Patten, T., Pelton, R., and Cranston, E. D. (2015). Synergistic Stabilization of Emulsions and Emulsion Gels with Water-Soluble Polymers and Cellulose Nanocrystals. *ACS Sustain. Chem. Eng.* 3, 1023–1031. doi:10.1021/acssuschemeng.5b00194

Huan, S., Mattos, B. D., Ajdary, R., Xiang, W., Bai, L., and Rojas, O. J. (2019). Two-Phase Emulgels for Direct Ink Writing of Skin-Bearing Architectures. *Adv. Funct. Mater.* 29, 1902990. doi:10.1002/adfm.201902990

Huang, B., He, H., Meng, S., and Jia, Y. (2019). Optimizing 3D Printing Performance of Acrylonitrile-butadiene-styrene Composites with Cellulose Nanocrystals/silica Nanohybrids. *Polym. Int.* 68, 1351–1360. doi:10.1002/pi.5824

Jiang, J., Oguzlu, H., and Jiang, F. (2021). 3D Printing of Lightweight, Super-strong yet Flexible All-Cellulose Structure. *Chem. Eng. J.* 405, 126668. doi:10.1016/j.cej.2020.126668

Jiménez Saelices, C., and Capron, I. (2018). Design of Pickering Micro- and Nanoemulsions Based on the Structural Characteristics of Nanocelluloses. *Biomacromolecules* 19, 460–469. doi:10.1021/acs.biomac.7b01564

Jiménez Saelices, C., Save, M., and Capron, I. (2019). Synthesis of Latex Stabilized by Unmodified Cellulose Nanocrystals: The Effect of Monomers on Particle Size. *Polym. Chem.* 10, 727–737. doi:10.1039/c8py01575a

Kalashnikova, I., Bizot, H., Cathala, B., and Capron, I. (2011). New Pickering Emulsions Stabilized by Bacterial Cellulose Nanocrystals. *Langmuir* 27, 7471–7479. doi:10.1021/la200971f

Kangas, H., Lahtinen, P., Sneck, A., Saariaho, A.-M., Laitinen, O., and Hellén, E. (2014). Characterization of Fibrillated Celluloses. A Short Review and Evaluation of Characteristics with a Combination of Methods. *Nord. Pulp Paper Res. J.* 29, 129–143. doi:10.3183/npprj-2014-29-01-p129-143

Kedzior, S. A., Dubé, M. A., and Cranston, E. D. (2017). Cellulose Nanocrystals and Methyl Cellulose as Costabilizers for Nanocomposite Latexes with Double Morphology. *ACS Sustain. Chem. Eng.* 5, 10509–10517. doi:10.1021/acssuschemeng.7b02510

Kedzior, S. A., Gabriel, V. A., Dubé, M. A., and Cranston, E. D. (2020). Nanocellulose in Emulsions and Heterogeneous Water-Based Polymer Systems: A Review. *Adv. Mater.* 33, 2002404. doi:10.1002/adma.202002404

Klemm, D., Kramer, F., Moritz, S., Lindström, T., Ankerfors, M., Gray, D., et al. (2011). Nanocelluloses: A New Family of Nature-Based Materials. *Angew. Chem. Int. Ed.* 50, 5438–5466. doi:10.1002/anie.201001273

Lam, S., Velikov, K. P., and Velev, O. D. (2014). Pickering Stabilization of Foams and Emulsions with Particles of Biological Origin. *Curr. Opin. Colloid Interf. Sci.* 19, 490–500. doi:10.1016/j.cocis.2014.07.003

Li, L., Chen, Y., Yu, T., Wang, N., Wang, C., and Wang, H. (2019). Preparation of Polylactic acid/TEMPO-Oxidized Bacterial Cellulose Nanocomposites for 3D Printing via Pickering Emulsion Approach. *Composites Commun.* 16, 162–167. doi:10.1016/j.coco.2019.10.004

Li, Y., Liu, X., Zhang, Z., Zhao, S., Tian, G., Zheng, J., et al. (2018). Adaptive Structured Pickering Emulsions and Porous Materials Based on Cellulose Nanocrystal Surfactants. *Angew. Chem. Int. Ed.* 57, 13560–13564. doi:10.1002/anie.201808888

Mabrouk, A. B., Salon, M. C. B., Magnin, A., Belgacem, M. N., and Boufi, S. (2014). Cellulose-based Nanocomposites Prepared via Mini-Emulsion Polymerization: Understanding the Chemistry of the Nanocellulose/matrix Interface. *Colloids Surf. A: Physicochemical Eng. Aspects* 448, 1–8. doi:10.1016/j.colsurfa.2014.01.077

Minas, C., Carnelli, D., Tervoort, E., and Studart, A. R. (2016). 3D Printing of Emulsions and Foams into Hierarchical Porous Ceramics. *Adv. Mater.* 28, 9993–9999. doi:10.1002/adma.201603390

Mohan, D., Teong, Z. K., Bakir, A. N., Sajab, M. S., and Kaco, H. (2020). Extending Cellulose-Based Polymers Application in Additive Manufacturing Technology: A Review of Recent Approaches. *Polymers* 12, 1876. doi:10.3390/POLYM12091876

Moreira, G., Fedeli, E., Ziarelli, F., Capitani, D., Mannina, L., Charles, L., et al. (2015). Synthesis of Polystyrene-Grafted Cellulose Acetate Copolymers via Nitroxide-Mediated Polymerization. *Polym. Chem.* 6, 5244–5253. doi:10.1039/c5py00752f

Murphy, C. A., and Collins, M. N. (2018). Microcrystalline Cellulose Reinforced Polylactic Acid Biocomposite Filaments for 3D Printing. *Polym. Compos.* 39, 1311–1320. doi:10.1002/pc.24069

Nasatto, P., Pignon, F., Silveira, J., Duarte, M., Noseda, M., and Rinaudo, M. (2015). Methylcellulose, a Cellulose Derivative with Original Physical Properties and Extended Applications. *Polymers* 7, 777–803. doi:10.3390/polym7050777

Nikfarjam, N., Taheri Qazvini, N., and Deng, Y. (2015). Surfactant Free Pickering Emulsion Polymerization of Styrene in W/o/w System Using Cellulose Nanofibrils. *Eur. Polym. J.* 64, 179–188. doi:10.1016/j.eurpolymj.2015.01.007

Ougiya, H., Watanabe, K., Morinaga, Y., and Yoshinaga, F. (1997). Emulsion-stabilizing Effect of Bacterial Cellulose. *Biosci. Biotechnol. Biochem.* 61, 1541–1545. doi:10.1271/bbb.61.1541

Ramsden, W. (1904). Separation of Solids in the Surface-Layers of Solutions and 'suspensions' (Observations on Surface-Membranes, Bubbles, Emulsions, and Mechanical coagulation).-Preliminary Account. *Proc. R. Soc. Lond.* 72, 156–164. doi:10.1098/rspl.1903.0034

Rees, A., Powell, L. C., Chinga-Carrasco, G., Gethin, D. T., Syverud, K., Hill, K. E., et al. (2015). 3D Bioprinting of Carboxymethylated-Periodate Oxidized Nanocellulose Constructs for Wound Dressing Applications. *Biomed. Res. Int.* 2015, 1–7. doi:10.1155/2015/925757

Sommer, M. R., Alison, L., Minas, C., Tervoort, E., Rühs, P. A., and Studart, A. R. (2017). 3D Printing of Concentrated Emulsions into Multiphase Biocompatible Soft Materials. *Soft Matter* 13, 1794–1803. doi:10.1039/C6SM02682F

Tammelin, T., Hippi, U., and Salminen, A. (2013). *Method for the Preparation of Nfc Films on Supports*. W.O. Patent No. 2013060934A2. Available at: https://patents.google.com/patent/WO2013060934A2/en.

Tenhunen, T.-M., Peresin, M. S., Penttilä, P. A., Pere, J., Serimaa, R., and Tammelin, T. (2014). Significance of Xylan on the Stability and Water Interactions of Cellulosic Nanofibrils. *Reactive Funct. Polym.* 85, 157–166. doi:10.1016/j.reactfunctpolym.2014.08.011

Voisin, H. P., Gordeyeva, K., Siqueira, G., Hausmann, M. K., Studart, A. R., and Bergström, L. (2018). 3D Printing of Strong Lightweight Cellular Structures Using Polysaccharide-Based Composite Foams. *ACS Sustain. Chem. Eng.* 6, 17160–17167. doi:10.1021/acssuschemeng.8b04549

Wang, J., Chiappone, A., Roppolo, I., Shao, F., Fantino, E., Lorusso, M., et al. (2018). All-in-One Cellulose Nanocrystals for 3D Printing of Nanocomposite Hydrogels. *Angew. Chem. Int. Ed.* 57, 2353–2356. doi:10.1002/anie.201710951

Wang, J., Gao, H., Hu, Y., Zhang, N., Zhou, W., Wang, C., et al. (2021). 3D Printing of Pickering Emulsion Inks to Construct poly(D,L-lactide-co-trimethylene Carbonate)-Based Porous Bioactive Scaffolds with Shape Memory Effect. *J. Mater. Sci.* 56, 731–745. doi:10.1007/s10853-020-05318-7

Werner, A., Schmitt, V., Sèbe, G., and Héroguez, V. (2017). Synthesis of Surfactant-free Micro- and Nanolatexes from Pickering Emulsions Stabilized by Acetylated Cellulose Nanocrystals. *Polym. Chem.* 8, 6064–6072. doi:10.1039/c7py01203a

Winuprasith, T., and Suphantharika, M. (2015). Properties and Stability of Oil-In-Water Emulsions Stabilized by Microfibrillated Cellulose from Mangosteen Rind. *Food Hydrocolloids* 43, 690–699. doi:10.1016/j.foodhyd.2014.07.027

Zhang, Y., Karimkhani, V., Makowski, B. T., Samaranayake, G., and Rowan, S. J. (2017). Nanoemulsions and Nanolatexes Stabilized by Hydrophobically Functionalized Cellulose Nanocrystals. *Macromolecules* 50, 6032–6042. doi:10.1021/acs.macromol.7b00982

Conflict of Interest: MG, KSK, AM, TV, and TT are employed by VTT Technical Research Centre of Finland Ltd.

The remaining authors declare that the research was conducted in the absence of any commercial or financial relationships that could be construed as a potential conflict of interest.

Publisher's Note: All claims expressed in this article are solely those of the authors and do not necessarily represent those of their affiliated organizations, or those of the publisher, the editors and the reviewers. Any product that may be evaluated in this article, or claim that may be made by its manufacturer, is not guaranteed or endorsed by the publisher.